

Global regularities in integrated galaxy spectra

Laerte Sodré Jr.^{1*} & Héctor Cuevas^{1†}

¹*Departamento de Astronomia, Instituto Astronômico e Geofísico da USP, Av. Miguel Stefano 4200, 04301-904 São Paulo, Brazil*

6 September 2018

ABSTRACT

We have investigated some statistical properties of integrated spectra of galaxies from Kennicutt (1992a) spectrophotometric atlas. The input for the analysis are galaxy spectra sampled in 1300 bins between 3750 Å and 6500 Å. We make use of Principal Component Analysis (PCA) to analyse the 1300-dimensional space spanned by the spectra. Their projection onto the plane defined by the first two principal components, the principal plane, shows that normal galaxies are in a quasi-linear sequence that we call spectral sequence. We show that the spectral sequence is closely related to the Hubble morphological sequence. These results are robust in the sense that the reality of the spectral sequence does not depend on data normalization. The existence of this sequence suggests that a single parameter may describe the spectrum of normal galaxies. We have investigated this hypothesis with Bruzual & Charlot (1995) models of spectral evolution. We show that, for single age models (15 Gyr), the spectral sequence can be parametrized by the characteristic star formation time-scales of the different morphological types. By examining the projection of evolutionary tracks of normal galaxies onto the principal plane, we verify that the spectral sequence is also an evolutive sequence, with galaxy spectra evolving from later to earlier spectral types. Considering the close correspondence between the spectral and morphological sequences, this lead us to speculate that galaxies may evolve morphologically along the Hubble sequence, from Sm/Im to E.

Key words: galaxies: general - classification - evolution - methods: statistical

1 INTRODUCTION

Normal galaxies tend to present great morphological regularities, which allow us to classify them along the Hubble sequence (Hubble 1926, Sandage 1961). The integrated spectra of nearby galaxies also show remarkable regularities. Their general properties have been recently discussed by Kennicutt (1992a,b), who has shown that normal galaxies have spectra that progress smoothly with the morphological type. Since the integrated spectrum of a galaxy represents a weighted mean in luminosity of the stellar populations that make it up, these results indicate that galaxies of same morphological type tend to have similar stellar populations, what provides the basis for a spectral classification of galaxies (Humason 1936, Morgan & Mayall 1957).

We present here a study of Kennicutt’s (1992a) spectrophotometric atlas, looking for global regularities in the

integrated spectra of galaxies. This is done with a standard statistical technique, Principal Component Analysis (PCA). PCA has previously been applied to the analysis and objective classification of spectra. Francis et al. (1992) have carried out a study of a large sample of QSO spectra, developing a quantitative classification scheme based on the first three principal components. Sodré & Cuevas (1994) have analysed a set of 24 normal galaxies from Kennicutt’s atlas, concluding that most of the variance present in their integrated optical spectra is due to their morphological differences. They have shown that these spectra may be parametrized by the morphological type, what allows a quantitative galaxy classification based on integrated spectra. Connolly et al. (1995) have studied the continuum spectra of the central regions of ten galaxies, covering a wavelength range from 1200Å to 1μm, also finding that ordinary galaxy spectra can be described by a one-parameter family. Folkes, Lahav & Maddox (1996) have used a combination of PCA and artificial neural networks for automated classification of galaxies from low signal-to-noise spectra.

* e-mail: laerte@astro1.iagusp.usp.br

† e-mail: hcuevas@astro1.iagusp.usp.br

Here we describe each spectrum by a point in a high-dimensional space where each dimension is the flux at each wavelength. We then apply PCA to obtain a suitable projection of the spectra onto a plane. This is done by identifying the orthogonal combinations of the variables with maximum variance, the ‘principal components’. Such a projection provides a synthetic view of the data space, allowing to investigate correlations between the spectra.

The plan of this paper is as follows. In section 2 we describe our input data, taken from Kennicutt’s atlas, and a data subset containing only normal galaxies. Some aspects of principal component analysis that are useful for the study presented here are reviewed in section 3. In this section we also discuss data normalization and scaling, since it is well known that it affects the output of PCA. The results of the application of PCA to all galaxies, as well as to the subset of normal galaxies, are presented in section 4 and discussed in section 5. Finally, section 6 summarises our conclusions.

2 THE DATA

The 55 integrated spectra investigated here are from Kennicutt’s (1992a) spectrophotometric atlas of galaxies. Most of the observations cover the wavelength range between 3650 Å and 7100 Å, with 5 - 8 Å resolution. To avoid incompleteness in the spectral coverage, we analyse here the rest-frame wavelength interval 3750 - 6500 Å. This spectral range was then uniformly re-sampled with 1300 bins, in order to approximately preserve the original bin width. The spectra in the atlas are normalized to unity at 5500 Å, implying that we are not taking into account any dependence with galaxy luminosity. We discuss below other normalizations and their effect on the results.

We have analysed two sets of data, one containing all galaxies (*AGS*), and a subset of *AGS* with normal galaxies only (*NGS*). The sample of normal galaxies contains 23 objects and covers the Hubble sequence from E to Im, avoiding objects with any evidence of peculiarity (e.g. AGNs, starbursts, mergers). The galaxies in this set are: NGC3379 (E0), NGC4472 (E1/S0), NGC4648 (E3), NGC4889 (E4), NGC3245 (S0), NGC3941 (SB0/a), NGC4262 (SB0), NGC5866 (S0), NGC1357 (Sa), NGC2775 (Sa), NGC3368 (Sab), NGC3623 (Sa), NGC1832 (SBb), NGC3147 (Sb), NGC3627 (Sb), NGC4775 (Sc), NGC5248 (Sbc), NGC6217 (SBbc), NGC2903 (Sc), NGC4631 (Sc), NGC6181 (Sc), NGC6643 (Sc), and NGC4449 (Sm/Im). Although small, the *NGS* allows us to explore the connection between normal galaxy spectra and morphology.

3 PRINCIPAL COMPONENT ANALYSIS

3.1 General Principles

Suppose we have a sample of N integrated spectra of galaxies, all covering the same rest-frame wavelength range. Each spectrum is described by a M -dimensional vector \mathbf{X} containing the galaxy flux at M uniformly sampled wavelengths. Let

\mathcal{S} be the M -dimensional space spanned by the ‘spectral’ vectors \mathbf{X} . An integrated spectrum, then, is a point in \mathcal{S} -space, and the spectra in the sample form a cloud of points in \mathcal{S} . If the spectral vectors of normal galaxies are indeed correlated with their morphology, one would expect that these points would be arranged more or less along a line, mimicking the Hubble morphological sequence. It is impossible, of course, to visualize how the data is distributed in high-dimensional spaces, like the 1300-dimensional spectral space discussed in next section. An alternative is to employ some technique for dimension reduction by projecting the data in, say, two dimensions.

Here we analyse the data with a standard technique, Principal Component Analysis (PCA). It is also known as Hotelling transform, or discrete Karhunen-Loève transform, but we call it PCA because this designation is more often used in Astronomy (e.g. Murtagh & Heck 1987 and references therein).

PCA is an orthogonal transformation that allows building more compact linear combinations of the data that are optimal with respect to the mean square error criterion. A detailed description of PCA can be found in several books on statistics or pattern recognition (e.g. Kendall 1975, Fukunaga 1990), as well as in the astronomical literature (e.g. Brosche 1973, Whitney 1983, Efstathiou & Fall 1984, Lahav et al. 1996). Here we restrict ourselves to a short outline of the procedure, emphasizing only the aspects that are relevant for our analysis.

Consider a set of N objects (galaxies) each with M features (flux at M given wavelengths). Let x_{ij} be the spectrum of the i -th object, i.e., it is the flux (or a scaled version of it, see below) at the j -th wavelength. It is often more useful to do the analysis with a pre-processed version of the data. For example, it is convenient to subtract the sample mean from each spectrum. This is equivalent to put the origin of the coordinate system at the barycentre of the data in the spectral space \mathcal{S} . It may be interesting, additionally, to re-scale each variable to unit variance. The first case is analogous to PCA of the covariance matrix, while the second is the same as PCA of the correlation matrix.

Let us then assume that the spectral vectors \mathbf{X} have zero mean. The covariance matrix of the data in this case is

$$C_{jk} = \frac{1}{N-1} \sum_{i=1}^N x_{ij}x_{ik} \quad (1)$$

Now, let us consider a new vector, \mathbf{Y} , which is a transformed version of \mathbf{X} , given by

$$\mathbf{Y} = \mathbf{A}\mathbf{X} \quad (2)$$

where \mathbf{A} is a $M \times M$ matrix whose rows are the eigenvectors of the covariance matrix \mathbf{C} .

This transform has several interesting properties. The covariance matrix of \mathbf{Y} is diagonal, with elements equal to the eigenvalues λ_k of \mathbf{A} . This means that the transformed vector components y_k are uncorrelated. Additionally, each eigenvalue λ_k is equal to the variance of the k -th element of \mathbf{Y} . Since \mathbf{A} is a real and symmetric matrix, its inverse is equal to the transpose, $\mathbf{A}^{-1} = \mathbf{A}'$. Then, it follows that \mathbf{X} can be reconstructed from \mathbf{Y} by using the relation

$$\mathbf{X} = \mathbf{A}'\mathbf{Y} \quad (3)$$

Suppose, however, that instead of using all the M components of \mathbf{Y} , we form a new matrix, \mathbf{A}_K , from the K eigenvectors corresponding to the K largest eigenvalues. The \mathbf{Y} vectors will then be K -dimensional and the reconstruction will no longer be exact. Let

$$\hat{\mathbf{X}} = \mathbf{A}'_K\mathbf{Y} \quad (4)$$

represent the approximation of \mathbf{X} obtained with the transformation matrix \mathbf{A}_K . It can be shown that the mean square error between \mathbf{X} and $\hat{\mathbf{X}}$ is given by

$$\mathcal{E} = \sum_{j=1}^M \lambda_j - \sum_{j=1}^K \lambda_j = \sum_{j=K+1}^M \lambda_j \quad (5)$$

This equation indicates that the reconstruction is exact if $K = M$. Also, for a given K , the error is minimized by selecting the eigenvectors associated with the K largest eigenvalues. Thus, the PCA transform is optimal in the mean square error sense.

Note that, contrarily to most implementations of PCA, here we do not re-normalize each transformed component by its corresponding $\lambda_k^{1/2}$, since this gives unit variance along the new axis, changing the metric of the transformed space.

The PCA transform has an important difference when compared to other orthogonal transforms: the basis vectors in ordinary orthogonal transforms (e.g. Fourier) are fixed, while in PCA they are the eigenvectors of the covariance matrix and, hence, they are data dependent.

The main body of this paper contains the analysis and discussion of the projected distribution of the spectra onto the plane (y_1, y_2) defined by the two first components of \mathbf{Y} . We call it the *principal plane*. The first principal component is taken to be along the direction in the M -dimensional spectral space with the maximum variance. The second principal component is constrained to lie in the subspace perpendicular to the first and, within that subspace, it is also taken along the direction with the maximum variance. Then, the principal plane is the plane that contains the maximum variance in the spectral space. In this sense it is the most informative plane contained in the data space.

3.2 Data Scaling

It is well known that the set of orthonormal coordinates resulting from an application of PCA is affected by the scaling of the data, and then the projection of the spectra onto the plane defined by the first two components is different for distinct data normalizations. The problem, here, is that the scaling may affect differently lines and continuum.

Consider, first, the normalization of the spectra. Results are different if the spectra are set to unit at 5500\AA , $f_{5500} = 1$, as they appear in Kennicutt's atlas, or if they are normalized to have the same mean flux within the wavelength range of interest, like in the analysis of Francis et al. (1992). Connolly et al. (1995) normalize each spectrum to unit norm, $\sum_{\lambda} f_{\lambda}^2 = 1$, and notice that the results are similar to the latter case above. The coefficients of the expansion, in this case, are direction cosines (e.g. Whitmore

Table 1. Percentage of the variance explained by the first two principal components

| method | sample | cumulative variance (%) |
|-------------|------------|-------------------------|
| covariance | <i>NGS</i> | 94.6 |
| | <i>AGS</i> | 93.1 |
| correlation | <i>NGS</i> | 86.5 |
| | <i>AGS</i> | 85.0 |

1984), and the spectra are distributed now onto the surface of a hypersphere of unit radius in the spectral space. Here we consider only the normalization of the spectra to the same mean flux, $\sum_{\lambda} f_{\lambda} = 1$. We have repeated the analysis with the other normalizations, verifying that they do not affect our main results.

As discussed in the previous section, the data is usually pre-processed before the analysis. Flux values at each wavelength can be scaled to zero mean (which we call covariance method) or to zero mean and unity variance (correlation method). The variance in the lines and continuum are equal in this last case. In order to control the effects due to scaling, we have applied both methods to the analysis of our data sets. It is worth pointing out, as we shall see, that our results are also invariant to the different data scaling, because the linear nature of the transform considered here preserves correlations between variables, independent of scaling (e.g. Francis et al. 1992).

4 RESULTS

We have applied PCA to a sample containing the spectra of all galaxies in Kennicutt's atlas (set *AGS*), as well as to a subsample comprising only normal galaxies (set *NGS*). The data was scaled before the analysis according to one of the procedures discussed above.

We consider first the compression achieved by the two transformed components (y_1, y_2) . The results are summarized in Table 1, which gives the cumulative fraction of the variance explained by these components for the two data sets, and for different scalings. We notice that there are not significant differences between the two sets. With the covariance method, $\sim 93 - 95\%$ of the total variance is described by the two first terms of the expansion. For the analysis with the correlation matrix, the cumulative variance is lower, but at least $\sim 85\%$ of the data variance is contained in two components now.

4.1 Analysis of the normal galaxies set (*NGS*)

Figure 1 shows the projection of the spectra of the *NGS* onto their principal plane. The most remarkable aspect in this figure is that the projected spectra of almost all galaxies are arranged along a quasi-linear sequence which we shall call *spectral sequence*. There are some outliers of the sequence for the covariance method (figure 1a), corresponding mainly

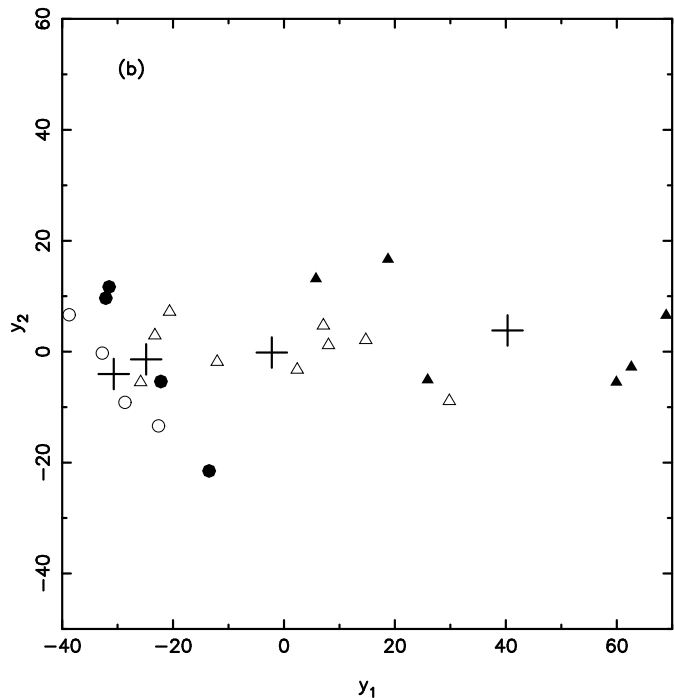
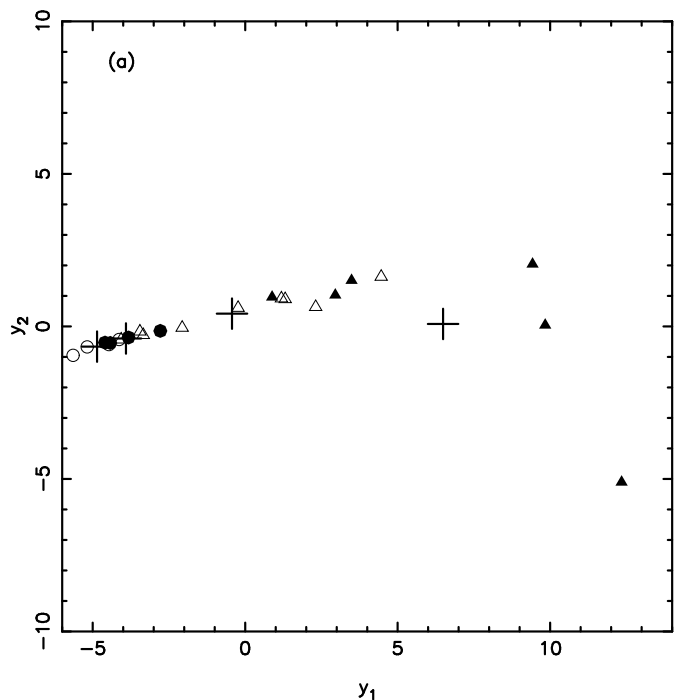


Figure 1. Projection of the spectra of the \mathcal{NGS} onto the principal plane: (a) covariance method; (b) correlation method. Different symbols correspond to different morphological types: E (open circles), S0 (filled circles), Sa-Sbc (open triangles), Sc-Im (filled triangles). Also shown in the figure are the projections of the mean spectra of these 4 morphological groups (crosses): E, S0, Sa-Sbc and Sc-Im (from left to right).

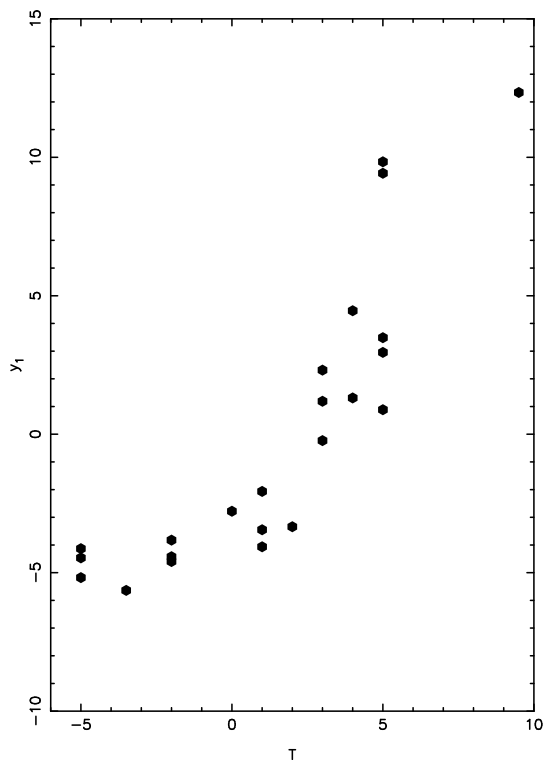


Figure 2. The first principal component, y_1 , versus T -types for the \mathcal{NGS} and the covariance method.

to late-type galaxies. For instance, the point with largest value of y_1 in figure 1 corresponds to the Sm/Im galaxy NGC4449. This is due, at least partially, to the ‘nebular’ nature of the spectrum of this galaxy (see section 4.3). Note that the Magellanic irregulars in the atlas are completely dominated by young stars and HII regions, and their spectra may not be representative of this class (Kennicutt 1992a). The sequence width is relatively larger for the correlation method (figure 1b), but even in this case it is clearly defined (the ratio between the standard deviations of y_1 and y_2 is $(\lambda_1/\lambda_2)^{1/2} \simeq 3.7$).

Most of the variance in the \mathcal{NGS} seems to be due to the morphological mix of the sample. We also show in figure 1 the projection of the mean spectra of 4 morphological groups (E, S0, Sa-Sbc, Sc-Im) onto the principal plane as crosses. Clearly, these groups are disposed along the spectral sequence keeping a ranking analogous to the Hubble sequence. It can be verified, however, that there is significant overlap of spectra of galaxies that are in distinct morphological groups. Indeed, an inspection of the spectra shows that there is a large scatter of spectral properties within each morphological group, and it is not difficult to find a *bona fide* galaxy of a given morphological type with a spectrum typical of galaxies of another type. Note that part of this discrepancy should be attributed also to the fuzzy nature of the morphological classification, as discussed by Naim et al. (1995) and Lahav et al. (1995), who found a dispersion of

1.8 T -units in the classification of a set of 830 APM galaxies by 6 experts.

In figure 2 we plot the first principal component y_1 versus the Hubble type, measured in the T -type system of RC3 (de Vaucouleurs et al. 1991), for the covariance method (results are similar for the correlation method). This plot presents a clear (non-linear) correlation between y_1 and T -type. In fact, Spearman's rank-order correlation coefficient between T -types and y_1 is high, 0.93 and 0.90 for the covariance and correlation methods, respectively, confirming that the correlation between these two quantities is significant. The same analysis done with the second principal component fails to show any significant correlation between T and y_2 . We conclude, then, that *the spectral sequence correlates strongly with the Hubble morphological sequence*. This result is relevant for galaxy classification since it allows to ascribe a type to a normal galaxy from its spectrum alone (e.g. by its value of y_1 or by its position along the spectral sequence).

Another point of interest contained in figure 2 is that the spectral variation, as measured by y_1 , is slow from E to Sab, increasing quickly for later types. This result also is independent of the data scaling, and reveals that the spectral distance between E ($T=-5$) and Sab ($T=2$) galaxies is smaller than between Sb ($T=3$) and Sc ($T=5$). Kennicutt (1992a) arrived at the same conclusion, arguing that unless one were able to measure the blue continuum colours or [OII] λ 3727 emission line to high accuracy, it would be difficult to distinguish the spectrum of a Sa-Sb from an E-S0 galaxy. Figure 2 also shows that the variance of y_1 increases with T , indicating that late-type galaxies present a richer spectral variety than early-types, at least for the sample studied here.

4.2 Analysis of all galaxies (AGS)

Figure 3 shows the projection of the AGS spectra onto their principal plane for the covariance method. This set includes normal galaxies, AGN, starburst, and interacting or merging galaxies. Most of the variance, now, is due to two galaxies only: Mk59 and Mk71. They are Sm galaxies with spectra dominated by HII-region emission, and here too the nebular nature of their spectra as well as the faintness of their continuum seems to be the cause of their position in the figure. The point to be stressed, however, is that the normal galaxies are again disposed along a sequence. This is best seen in figure 3b, where we have zoomed out part of figure 3a. The projections resulting from the correlation method are shown in figure 4, and are qualitatively similar to those displayed in figure 3. The spectral sequence is clearly visible, what confirms that it is an intrinsic property of the integrated spectra of normal galaxies.

How are galaxies other than the normal ones distributed in the (y_1, y_2) plane? The answer now depends on the scaling and, for most types of peculiar galaxies, their location with respect to the normal galaxies varies from plot to plot in figures 3 and 4. An important exception are the starburst nuclei NGC3471, NGC5996 and NGC7714, which consistently fall over the Sc-Im region of the spectral sequence.

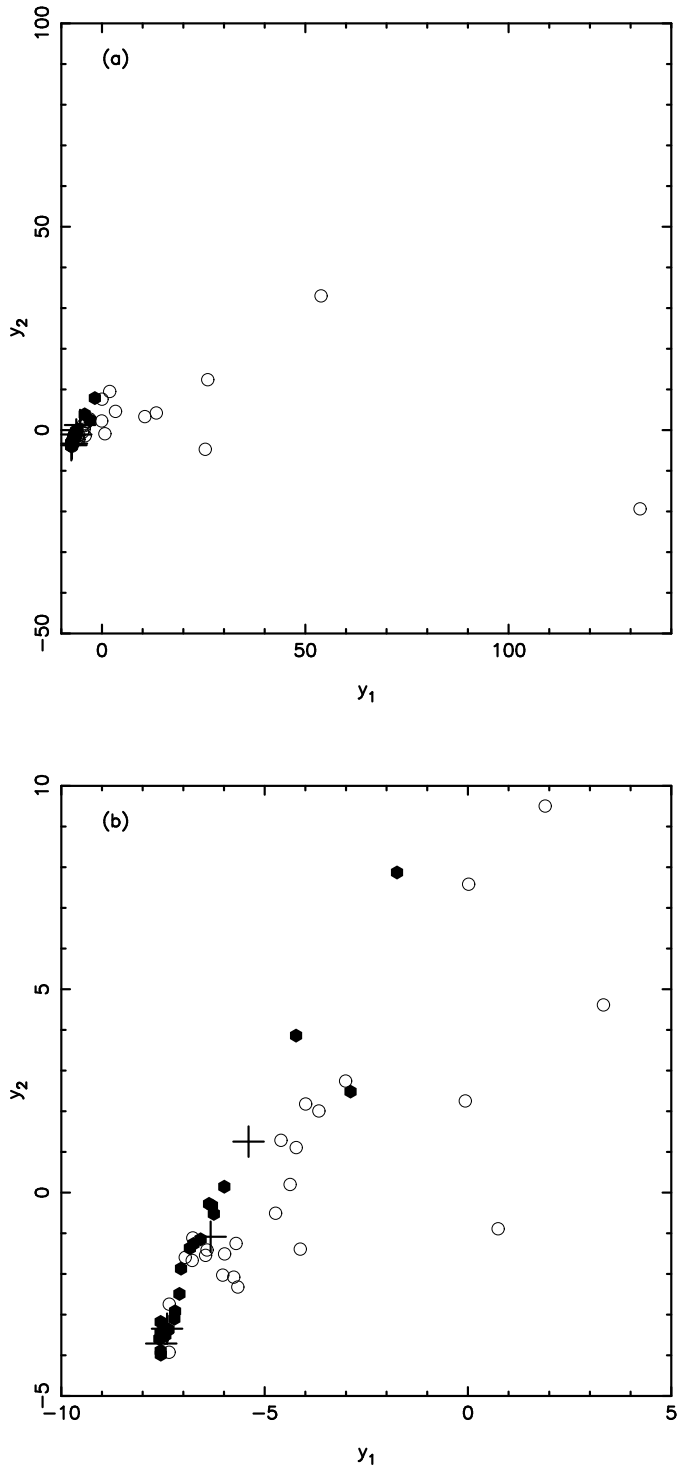


Figure 3. Projection of the spectra of AGS onto the principal plane for the covariance method. The projected spectra of normal galaxies are represented here as filled hexagons, while those of peculiar galaxies are shown as open circles. The mean spectra are represented by crosses (see caption of figure 1). Figure 3b is similar to 3a, but zoomed out to enhance the spectral sequence.

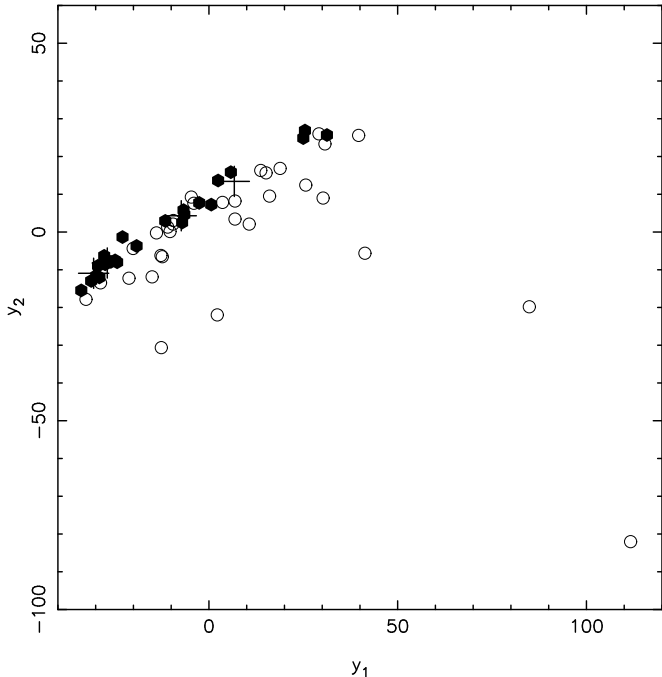


Figure 4. Same as figure 3a, but for the correlation method.

4.3 The nature of the principal components

PCA is a linear transform and then each principal component is a linear combination of the flux at all wavelengths. We plot in figure 5 the weights associated with each wavelength for the two first principal components for galaxies in the *NGS*. This figure is useful because it provides an insight on what determines y_1 and y_2 for each type of data scaling. Results for the *AGS* are similar.

Figure 5a shows the weights corresponding to y_1 for the covariance method. They are the components of the first eigenvector of the covariance matrix. The overall weight distribution is regular, being positive in the blue and decreasing to negative values for longer wavelengths. Blue galaxies, then, tend to have larger values of y_1 than the red ones. But large weights are associated with wavelengths of emission lines, mainly [OIII] $\lambda\lambda$ 4959,5007 and $H\beta$. This might lead one to suppose that y_1 is actually measuring the strength of these lines. To clarify this point, we repeated the analysis excluding small regions around the Balmer lines and

the [OIII] nebular lines. The projection of the galaxies onto their principal plane looks like that shown in figure 1b, with the two previous late-type outliers of figure 1a now disposed along the sequence. Note that most galaxies in the *NGS* present negligible or small emission at the wavelengths of the [OIII] lines and $H\beta$, and then the information carried by these wavelengths is proportional to the continuum flux at $\sim 5000\text{\AA}$. Galaxies with strong nebular spectrum will have larger values of y_1 because they tend to be bluer than the others and, mainly, because of the large and positive contribution of their line flux. We conclude that the information associated with the spectral sequence comes essentially from the continuum, with a significant contribution of emission lines, when present. This is confirmed by figure 5b, where it is shown the weights corresponding to y_2 . These weights are almost zero, except at the wavelengths close to the emission lines, where they present an oscillation. These oscillations act like a line detector as it computes a linear combination of differences between the flux at the line and the nearby continuum (adjacent continuum - line, actually): y_2 is near zero for spectra without emission lines, and negative for those where the lines are prominent. This explains the position of the outliers in figure 1a.

The covariance method preserves the differences between the continuum and the lines and then our result reveals that a large fraction of the variance of the sample is coming from wavelengths associated with $H\beta$ and the [OIII] nebular lines. In the correlation method, lines and continuum are put to the same variance, and the resulting weights are quite different, as shown in figures 5c and 5d. The continuum now provides a contribution to y_1 more significant than the emission lines. The distribution of the weights shows that y_1 is measuring the flux difference between the blue and red parts of a spectrum, with a non negligible contribution of some lines. The weights associated with y_2 in the correlation method are shown in figure 5d. Their behaviour is quite different from that shown in figure 5b for the covariance method. Now y_2 is essentially probing the wavelength interval between 4300\AA and 5200\AA . Then, to first order, y_1 is measuring a colour and y_2 the relative flux at $\sim 4750\text{\AA}$.

The discussion in this section reveals that the detailed interpretation of the principal components are quite dependent of the data set. At the same time, it indicates that is the continuum that gives the major contribution to the first component, but nebular emission may also be important.

4.4 Effect of the errors

The overall accuracy of the spectrophotometry of the galaxies in the atlas is $\sim 5\text{-}10\%$. To investigate the effect of these errors we have adopted the following procedure. For two normal galaxies, NGC3379 (E0) and NGC4631 (Sc), we produced 100 simulated spectra by adding Gaussian noise with standard deviation equal to 0.1 times the flux at each wavelength to the two observed spectra. For each data set and type of scaling, the simulated spectra were pre-processed and projected onto the principal plane. We have verified that the errors have more effect on the late-type galaxy spectrum than on the elliptical spectrum, due to the emission lines

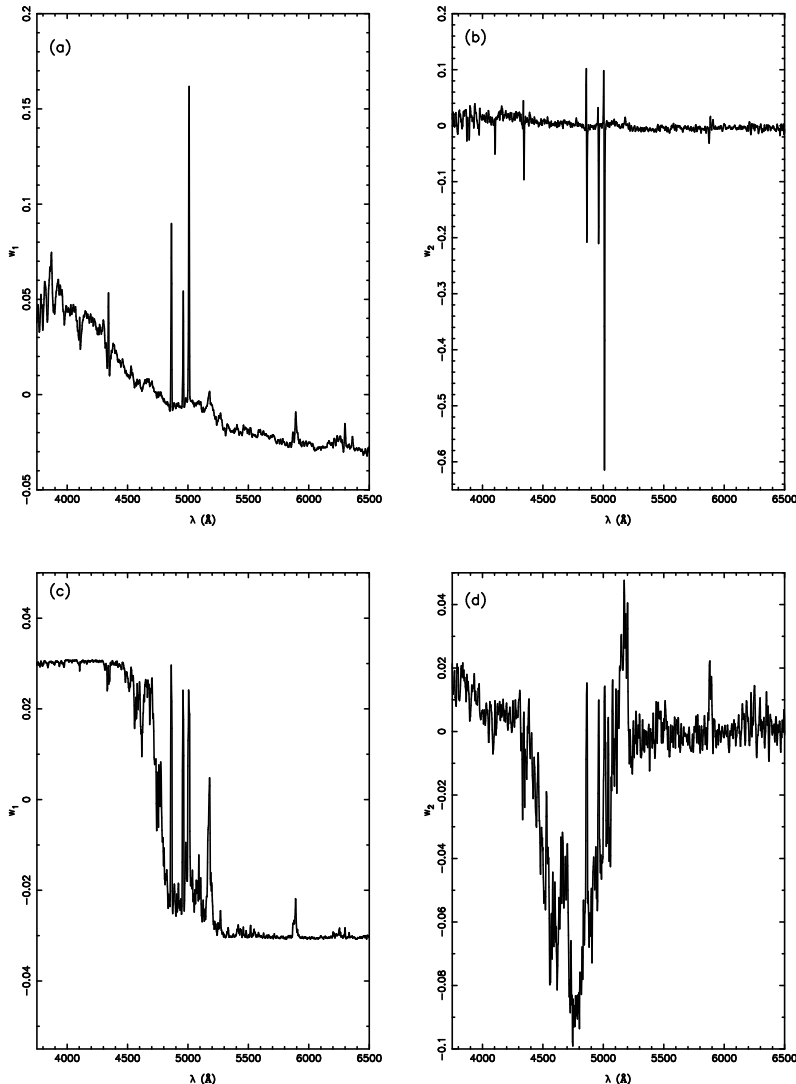


Figure 5. Weights (components of eigenvectors) associated to the principal components y_1 and y_2 for the \mathcal{NGS} : (a) y_1 , covariance method; (b) y_2 , covariance method; (c) y_1 , correlation method; (d) y_2 , correlation method.

present in the spectrum of the former object. Their effect on the results presented here are, however, negligible.

5 DISCUSSION

5.1 The spectral sequence

The results of the previous section allow us to conclude that the spectral sequence is real in the sense that the spectra of normal galaxies form a sequence in the spectral space. This result is robust because, as we have seen, it is independent of data normalization and scaling. Note that figures 1a and 3 represent projections of the same data space (for the covariance method) onto different planes: while in figure 1a the plane maximizes the variance of the \mathcal{NGS} , the principal

plane in figure 3 maximizes the variance of the \mathcal{AGS} . The same is true for figures 1b and 4 for the correlation method.

It is well known that several parameters related to spectra, like colours or spectral indices, correlate well with the Hubble sequence (e.g. Roberts & Haynes 1994). We had already noticed (Sodr e & Cuevas 1994) that in a data space defined by spectral parameters, like the amplitude of the 4000  break and the strength of the G band or the Mg2 index, the morphological types are distributed along a one-dimensional sequence. Our results here indicate that these empirical correlations are due to the global regularities present in galaxy spectra, illustrated here by the spectral sequence. It provides quantitative support for a one-dimensional description of the general properties of normal galaxies, like the Hubble morphological sequence. It also indicates that there is not a dividing line in spectral properties

between elliptical and spiral galaxies, and that lenticulars have spectra intermediate between those two morphological groups (c.f. figures 2-4).

The existence of the spectral sequence and its relation with the morphological sequence has been recognized by Connolly et al. (1995). They applied a procedure similar to ours to a sample of 10 composite spectra of the central regions of normal and starburst galaxies, each covering a wavelength range of 1200Å to 1μm. Interestingly, they found that their 10 spectra were disposed along a spectral sequence, in disagreement with our results, where the spectral sequence is defined only by the normal galaxies. This is due to two effects. First, they have removed the strongest nebular emission lines from the starburst spectra, decreasing the variance associated with the lines (c.f. section 4.3). Second, a visual examination of their spectra indicates that most of the variance, now, is coming from the UV continuum ($\lambda \lesssim 3000\text{Å}$), a region not included in our analysis. This discussion confirms how dependent of the input data the results of PCA are! Another point that is worth mentioning is that Connolly et al. (1995) found a curved spectral sequence, while in our study it is more or less linear. This is a consequence of their normalization by the scalar product, that projects the spectra onto the surface of a hypersphere in the spectral space.

Taken together, these results increase the robustness of the spectral sequence of normal galaxies, as it appears in all these analysis of galaxy spectra, irrespective of the wavelength interval, spectral resolution, or the detailed form of the input. Consequently, we expect that a study of a sample that includes, say, H α , will lead to the same general conclusions although the projection of the galaxies onto the new principal plane probably will be different.

The principal plane is convenient for classification of normal galaxies, because we can ascribe an objective spectral type to a normal galaxy from its position along the sequence. The spectra of peculiar galaxies, however, occupy positions in the principal plane that depend whether one uses the covariance or the correlation method, since the relative rôle of continuum and lines is different for each of the two scaling methods. Hence, the principal plane is not adequate for classification of non-normal galaxies, i.e., one needs more than just two dimensions to describe the general manifold of integrated spectra of galaxies.

An obvious advantage of spectral classification over morphological classification is that the former is more adequate to a quantitative approach than the latter. For instance, Folkes, Lahav & Maddox (1996) developed a method for galaxy classification from low signal-to-noise spectra typical of reshift surveys. They have simulated spectra of normal galaxies with the parameters of the 2dF Galaxy Redshift Survey. Using a combination of PCA and artificial neural networks, they show that it is necessary typically 8 principal components to describe normal noisy spectra and be able to classify them. Their results indicate that $\sim 95\%$ of the spectra are correctly classified in 5 morphological groups at $b_J = 19.7$, the limiting magnitude of the survey. Since they also used Kennicutt's data, their PCA results are very simi-

lar to ours, even noting that their sample of normal galaxies contains 3 galaxies more than ours.

5.2 Model spectra

The principal plane provides us with a useful tool to analyse spectra. We illustrate this point with the following exercise. The very existence of the spectral sequence, and its correlation with the Hubble sequence, indicates that one single parameter may be responsible for the integrated spectra of normal galaxies- and of the morphological sequence. For instance, Gallagher, Hunter & Tutukov (1984), Sandage (1986) and Ferrini & Galli (1988), suggest that several properties of the Hubble sequence can be explained by variations in the star formation rate of galaxies.

We have investigated this hypothesis with Bruzual & Charlot (1995, hereafter B&C) revised models of spectral evolution of galaxies (see also Bruzual & Charlot 1993). We have only considered models with a single parameter, the characteristic star formation time-scale of a galaxy, τ , where the SFR decreases with time as $\exp(-t/\tau)$. We assume a Salpeter IMF, with lower and upper mass limits equal to 0.1 and 125 M_\odot , respectively, and neglect gas recycling. Each model results in a spectrum sampled at 238 channels within the wavelength range of interest here. For consistency, we have computed the principal components of our two data sets using the same 238 channels of the theoretical spectra, instead of our 1300 previous wavelengths. The cumulative variance explained by the principal plane is not too affected by this reduction of spectral resolution. For the \mathcal{AGS} , it is now 93.7% and 86.0% for the covariance and correlation methods, respectively.

Let us first consider single age models (15 Gyr). In figure 6 we show, for several values of τ , the projection of the model spectra onto the principal plane defined by the galaxies in each of our two data sets. The model spectra overlap the spectral sequence for the two methods, although they tend to fall below the mean types for the correlation method. For each data set and normalization, the spectrum corresponding to a single instantaneous burst ($\tau = 0$, i.e., B&C model bc95-ssp-sp-1) falls just at the left extreme of the sequence. On the opposite extreme, the spectrum of a composite stellar population with constant star formation rate ($\tau = \infty$, i.e., model bc95-cons-sp-1), a simple model for irregular galaxies, is near the mean locus of Sc galaxies in the principal plane. Other values of τ are distributed along the sequence, between these two extremes. Figure 6 indicates that the parameter τ provides a good parametrization of the spectral sequence, from elliptical to irregular galaxies (although this seems not to be quite true for the correlation method applied to the \mathcal{NGS} , even in this case the results are satisfactory if one takes into account the simplicity of the models considered here). This result is in agreement with the conclusions of Kennicutt, Tamblyn & Congdon (1994), who have shown that the photometric properties of spiral galaxies along the Hubble sequence are predominantly due to changes in the star formation histories of disks, and only secondarily to changes in the bulge-to-disk ratio, which also varies systematically along the morphological sequence.

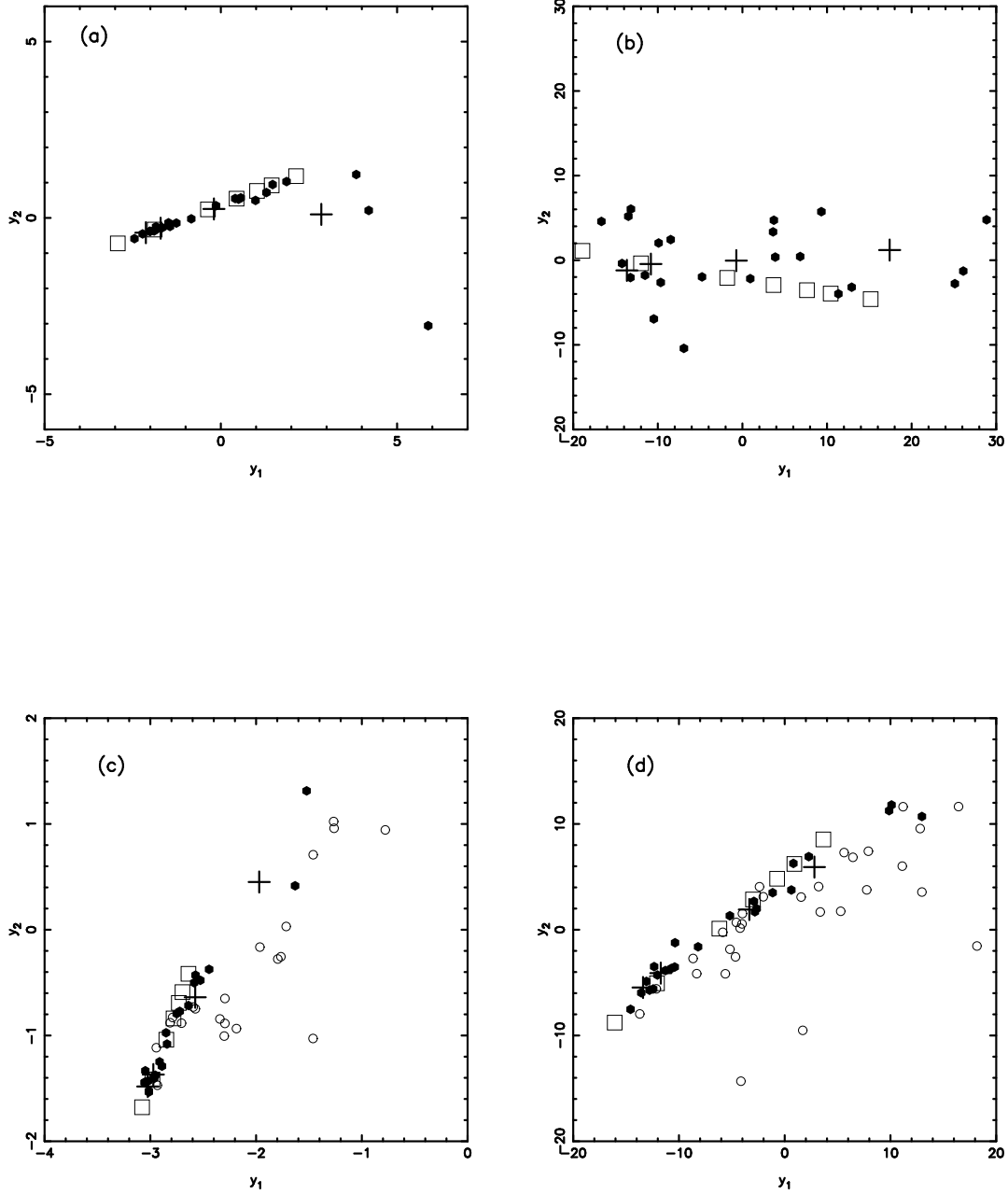


Figure 6. Projection of B&C model spectra for several values of the mean star formation time scale τ and age equal to 15 Gyr onto the principal plane: (a) \mathcal{NGS} , covariance method; (b) \mathcal{NGS} , correlation method; (c) \mathcal{AGS} , covariance method; (d) \mathcal{AGS} , correlation method. Model spectra are represented by open squares. They correspond, from left to right, to $\tau=0, 3, 5, 7, 10, 15$ and ∞ Gyr (see text for details). Other symbols have the same meaning as in figure 3. In figures 6c and 6d, only the part of the principal plane occupied by the spectral sequence is shown.

We plot in figure 7 evolutive tracks for the $\tau = 0$ and $\tau = \infty$ models, with galaxy ages running from 0 to 20 Gyr. The evolutive track of an instantaneous burst, for the covariance method, overlaps the spectral sequence, that is, its spectrum evolves from late to early-types along the sequence. The same is partially true for the constant star formation rate model, but in this case the oldest spectrum falls near the centroid of normal Sc galaxies. Hence, in the principal plane obtained with the covariance method, the spectral sequence not only characterizes the locus of normal galaxies but is almost coincident with their evolutionary tracks. Figure 7 also shows that, for the correlation method, these tracks present more structure, but the same evolutive trend holds. It is worth pointing out that these tracks correspond to very simple models, and ‘cosmic variance’, e.g. differences in the epoch of galaxy formation, IMF, SFR, metallicity, dust content, etc., may well lead to models able to cover all the spectral sequence. Note that these tracks do not explain why some galaxies are out of the spectral sequence. Although most of them probably have a more complex star formation history than the simple exponential decreasing star formation rate considered here, the main reason is that B&C spectra do not include nebular emission produced by HII regions, and hence they are not adequate to describe galaxies with spectra dominated by ongoing star formation, like Mk59 or Mk71.

5.3 On the nature of the Hubble sequence

Our results lead us to conclude that the spectral sequence is also an evolutive sequence, with galaxy spectra evolving from Magellanic irregulars to that of ellipticals. Consequently, we expect that the fraction of galaxies with late-type spectra should increase with redshift. It is well known that the fraction of blue objects increases with the redshift, as evidenced originally by the Butcher-Oemler (1978) effect in clusters (see Rakos & Schombert 1995 for a recent study) or by the dramatic excess (with respect to no-evolution models) in galaxy counts in faint blue magnitudes (see Ellis 1990 for a review). Additionally, recent observations with the HST have been able to show that these galaxies are mainly late-type spirals and irregulars (Glazebrook et al. 1995; Driver, Windhorst & Griffiths 1995).

We have seen that there is a close correspondence between the spectral and morphological sequences today, and that the spectral sequence is also an evolutive sequence. If we do not live in a special epoch in the history of the Universe, we may suppose that the spectral and morphological sequences have been always related. Then the Hubble sequence itself would be an evolutionary sequence, with galaxies evolving from Im to E! This is a speculation, of course, since our results refer to spectra and not to morphologies, and then the appearance of an E galaxy with age of 1 Gyr may be quite different of what is today an \sim Sc galaxy. But is worth noting that some recent works present evidence that the morphology of a normal galaxy may evolve from late to early types. For instance, Pfenniger, Combes & Martinet (1994) and Pfenniger, Martinet & Combes (1996) argue that this evolution may be driven by internal and external fac-

tors due to the likely coupling between dynamics and star formation. The key point is that dynamical process that actuate during a galaxy life- like formation and destruction of bars, mergers, close encounters, gas compression and/or stripping, etc.- tend to favour an increase of the spheroidal component at the expense of the disk, leading to a univocal sense of morphological evolution, from Sm to Sa. This sense of evolution also explains the morphological content of galaxy clusters, where most of galaxies are E or S0. The simplest explanation assumes that there is an infalling population of late-type galaxies (Sodré et al. 1989, Kauffmann 1995) that are transformed in E and S0 (as well as in dwarf ellipticals) in the hostile environment of the clusters. Moore et al. (1996) have recently proposed that frequent encounters at high speed among the galaxies in clusters (“galaxy harassment”) may be the driver of morphological transformations in these environments. This process may explain the Butcher-Oemler effect and the form of the blue objects observed in high-redshift clusters by the HST. Hierarchical models also indicate that galaxy morphology may well change as consequence of mergers and interactions (Baugh, Cole & Frenk 1996), although these models do not have yet enough resolution to address the question of evolution within spiral types. This scenario also suggests that the first galaxies should look more like faint gas rich irregular objects- in agreement with the inhomogeneous galaxy formation models of Baron & White (1987)- than the presumed bright precursors of today’s elliptical galaxies and bulges of spirals in the scenario devised by Eggen, Lynden-Bell & Sandage (1962).

Note that our results are consistent with this ‘nurture’ scenario, but they do not exclude by any means the ‘nature’ framework, where the morphology of a galaxy is already imprinted in the initial conditions at the moment of birth, with the galaxy spectrum evolving passively with time, without any significant morphological evolution. We hope that HST observations may be able to constrain the amount of morphological evolution of high redshift galaxies and help solving the long standing problem of the origin of the Hubble sequence.

6 CONCLUSIONS

We have applied PCA to the study of integrated spectra of galaxies. We have found useful to analyse the projected distribution of galaxy spectra onto the principal plane, defined as the plane in the data space that contains most of the data variance. We have shown that normal galaxies delineate a spectral sequence, which is related to the Hubble morphological sequence, i.e., the spectrum of normal galaxies changes smoothly from E to S0 to Sa, up to Sc and Im, without a gap between ellipticals and spirals. The spectral sequence in the principal plane is somewhat analogous to the main sequence in the HR diagram. The existence of the spectral sequence is independent of the data scaling and provides quantitative support for the Hubble morphological sequence.

The fact that normal galaxies form a one-dimensional spectral sequence may indicate that a single parameter controls their integrated spectra (and the Hubble sequence). With Bruzual & Charlot models we have shown that the

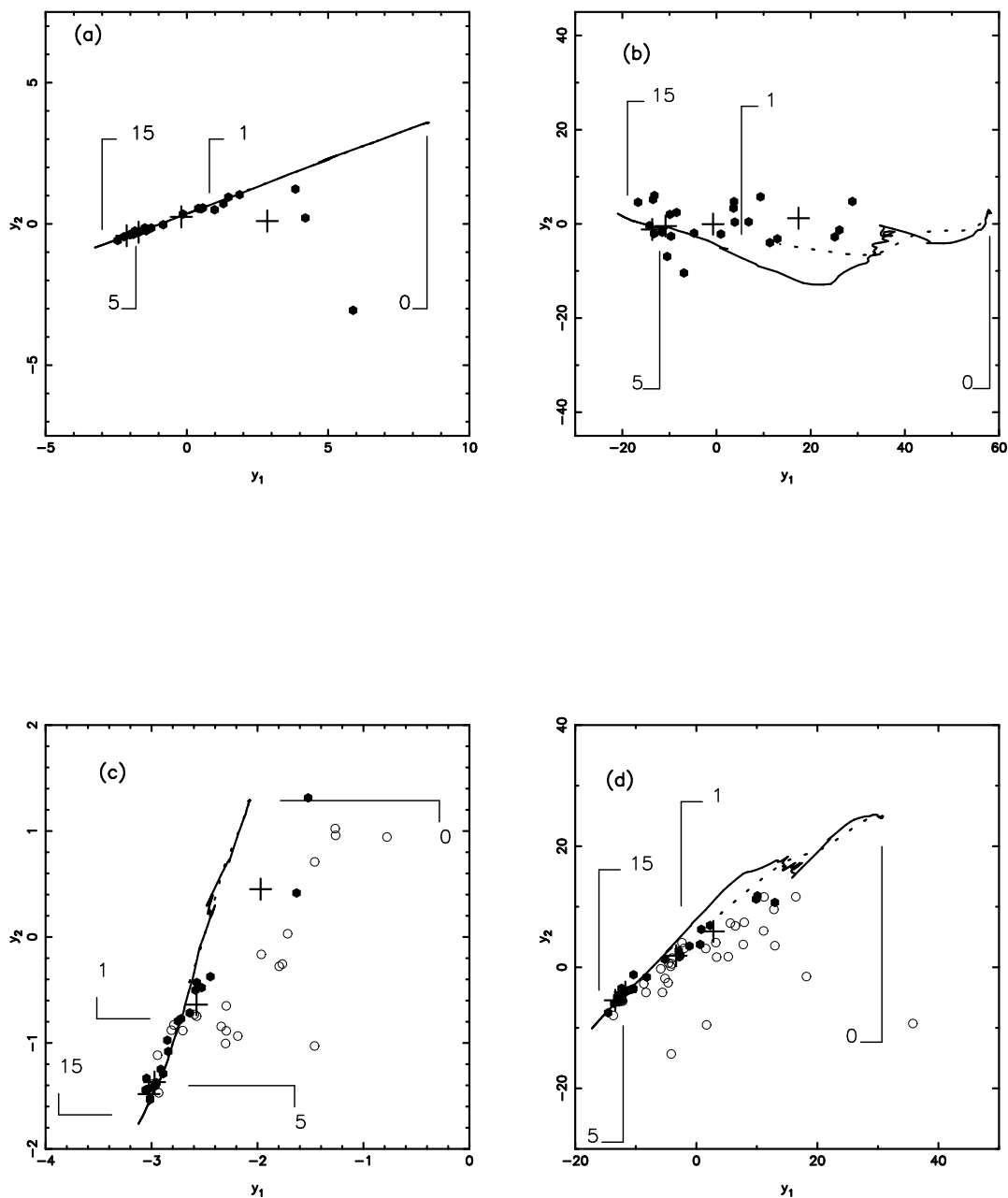


Figure 7. Projection of B&C evolutionary tracks for $\tau = 0$ (continuous line) and $\tau = \infty$ (dotted line) onto the principal plane: (a) \mathcal{NGS} , covariance method; (b) \mathcal{NGS} , correlation method; (c) \mathcal{AGS} , covariance method; (d) \mathcal{AGS} , correlation method. Symbols have the same meaning as in figure 3. The age (in Gyr) is indicated next to the tracks. Note that the track for $\tau = 0$ completely overlaps the track for $\tau = \infty$ in the covariance method (7a and 7c).

characteristic star formation time scale of galaxies provides a good parametrization of the spectral sequence. Additionally, the evolutionary tracks of normal galaxies, when projected onto the principal plane defined by the spectra of presently normal galaxies, overlap completely (for E galaxies) or partially (for late-type galaxies) the spectral sequence. This means that galaxy spectra evolve along the sequence, at least for the simple evolutionary models discussed here. Taking into account the close correspondence between the spectral and morphological sequences, our results are consistent with the hypothesis that galaxies may also evolve morphologically along the Hubble sequence, from Sm/Im to E.

It is worth noting that PCA is dependent of the data set, since the analysis is done over the covariance or correlation matrix of the data. As we have shown, however, our main results are robust in the sense that they are, in a large extent, independent of data scaling or spectral resolution. It will be interesting to repeat this analysis when richer samples, including high redshift galaxies, become publically available.

ACKNOWLEDGEMENTS

We are pleased to thank G. Bruzual and S. Charlot for making their galaxy isochrone synthesis spectral evolution library (GISSEL95) available to us, Ofer Lahav and Avi Naim for many discussions on PCA, and an anonymous referee for comments that allowed us to improve the paper. We also thank Eduardo Telles and Claudia Mendes de Oliveira for their help on the revision of this paper. The Kennicutt atlas was obtained from the Astronomical Data Center (ADC). This work benefited from the financial support provided by the Brazilian agencies FAPESP, CNPq, and CAPES.

REFERENCES

- Baron E., White S.D.M., 1987, *ApJ*, 322, 585
 Baugh C.M., Cole S., Frenk C.S., 1996, *MNRAS*, submitted
 Brosche P., 1973, *A&A*, 23, 259
 Bruzual G., Charlot S., 1993, *ApJ*, 405, 538
 Bruzual G., Charlot S., 1995, *Galaxy Isochrone Synthesis Spectral Evolution Library (GISSEL95)*
 Butcher H., Oemler A., 1978, *ApJ*, 219, 18
 Connolly A.J., Szalay A.S., Bershady M.A., Kinney A.L., Calzetti D., 1995, *AJ*, 110, 1071
 de Vaucouleurs, G., de Vaucouleurs A., Corwin Jr. H.G., Buta R., Paturel G., Fouqué P., 1991, *Third Reference Catalogue of Bright Galaxies*. Springer-Verlag, New York
 Driver S.P., Windhorst R.A., & Griffiths R.E., 1995, *ApJ*, 453, 48
 Efstathiou G., Fall S.M., 1984, *MNRAS*, 206, 453
 Eggen O., Lynden-Bell D., Sandage A., 1962, *ApJ*, 136, 748
 Ellis R.S., 1990, in Kron R.G., ed, *Evolution of the Universe of Galaxies*, A.S.P. Conference Series, Vol. 10, p248
 Ferrini F., Galli D., 1988, *A&A*, 195, 27
 Folkes S.R., Lahav O., Maddox S.J., 1996, *MNRAS*, submitted
 Francis P., Hewett P.C., Foltz C.B., Chafee F.H., 1992, *ApJ*, 398, 480
 Fukunaga K., 1990, *Statistical Pattern Recognition*. Academic Press, New York
 Gallagher J., Hunter D., Tutukov A., 1984, *ApJ*, 284, 544
 Glazebrook K., Ellis R.S., Santiago B., Griffiths R.E., 1995, *MNRAS*, 275, L19
 Hubble E., 1936, *The Realm of Nebulae*. Yale Univ. Press, New Haven
 Humason M.L., 1936, *ApJ*, 83, 18
 Kauffmann G., 1995, *MNRAS* 274, 153
 Kendall M., 1975, *Multivariate Analysis*. Griffin, London
 Kennicutt R.C., 1992a, *ApJS*, 79, 255
 Kennicutt R.C., 1992b, *ApJ*, 388, 310
 Kennicutt R.C., Tamblyn P., Congdon C.W., 1994, *ApJ*, 435, 22
 Lahav O., Naim A., Buta R.J., Corwin H.G., de Vaucouleurs G., Dressler A., Huchra J.P., van den Bergh S., Raychaudhury S., Sodré L., Storrie-Lombardi M.C., 1995, *Science*, 267, 859
 Lahav O., Naim A., Sodré L., Storrie-Lombardi M.C., 1996, *MNRAS*, submitted
 Moore B., Katz N., Lake G., Dressler A., Oemler A., 1996, *Nature*, 379, 613
 Morgan W.W., Mayall N.U., 1957, *PASP*, 69, 291
 Murtagh F., Heck A., 1987, *Multivariate Data Analysis*. D. Reidel, Dordrecht
 Naim A., Lahav O., Sodré L., Storrie-Lombardi M.C., 1995, *MNRAS*, 275, 567
 Pfenniger D., Combes F., Martinet L., 1994, *A&A*, 285, 79
 Pfenniger D., Martinet L., Combes F., 1996, preprint, astro-ph/9602139
 Rakos K.D., Schombert J.M., 1995, *ApJ*, 439, 47
 Roberts M.S., Haynes M.P., 1994, *ARA&A* 32,115
 Sandage A., 1961, *The Hubble Atlas of Galaxies*. Carnegie Institute of Washington, Washington, DC
 Sandage A., 1986, *A&A*, 161, 89
 Sodré L., Capelato H.V., Steiner J.E., Mazure A., 1989, *AJ* 97, 1279
 Sodré L., Cuevas H., 1994, *Vistas in Astron.*, 38, 287
 Whitmore B.C., 1984, *ApJ*, 278, 61
 Whitney C.A., 1983, *A&AS*, 51, 443